Electron-positron momentum density in TTF-TCNQ

Shoji Ishibashi
Electrotechnical Laboratory, 1-1-4 Umezono, Tsukuba, Ibaraki 305, Japan

Alfred A. Manuel and Ludger Hoffmann
Département de Physique de la Matière Condensée, Université de Genève, 24 quai E. Ansermet, CH-1211 Geneva 4, Switzerland

Klaus Bechgaard
Department of Solid State Physics, Risø National Laboratory, P.O. Box 49, DK-4000 Roskilde, Denmark
(Received 10 July 1996; revised manuscript received 18 September 1996)

We present measurements of the positron two-dimensional angular correlation of annihilation radiation (2D-ACAR) in TTF-TCNQ. We report also theoretical simulations of the 2D-ACAR in which the electron wave functions were expressed as TTF or TCNQ molecular orbitals obtained from self-consistent quantum chemical calculations. The positron wave function was calculated taking the charge transfer from TTF to TCNQ as a parameter. The best agreement with the experiment is obtained for a charge transfer of 0.7 electrons from the TTF to the TCNQ molecules. This is larger than the value of 0.55 obtained from a study of the Kohn anomaly. We investigate also the shape and position of the Fermi surface and conclude that a simple planar Fermi surface is consistent with our measurements. [S0163-1829(97)04104-0]

I. INTRODUCTION

The organic compound tetrathiofulvalinium tetracyanoquinodimethan (TTF-TCNQ) is the first synthesized organic conductor. It has been widely studied due to its quasi-one-dimensional conductivity. TTF-TCNQ has a monoclinic crystal structure (space group $P2_1/c$) with lattice parameters of $a=12.298$ Å, $b=3.819$ Å, $c=18.468$ Å, and $\beta=104.46°$.[1] It consists of homologous stacks of cations (TTF) and anions (TCNQ) along the b axis and shows one-dimensional metallic conductivity in this direction above 58 K.[2] This conductivity is due to a charge transfer between the two different types of molecules.

The Fermi surface is expected to be made of quasiplanar sheets as a consequence of the one dimensionality of the conductivity. The Kohn anomaly measurement has indirectly provided the position of these Fermi surfaces.[3] Usually, a de Haas–van Alphen, Shubnikov–de Haas, or angular-dependent magnetoresistance oscillation technique is applied in determining the morphology of Fermi surfaces in organic conductors.[4] These techniques, which require low-temperature measurements, are not available on TTF-TCNQ, since it becomes an insulator below 58 K.[2]

The positron annihilation 2D-ACAR (two-dimensional angular correlation of annihilation radiation) technique is recognized as a powerful tool to measure electronic structures in momentum space.[5] It provides 2D projections of the two-photon momentum density (TPMD), which corresponds to the electron momentum distribution as sampled by positrons. The Fermi-surface topology induces discontinuities in the TPMD. These discontinuities reflect accordingly in the 2D-ACAR distributions. The 2D-ACAR method can be used at any temperature to obtain direct information about the Fermi surface. This is a unique advantage for the study of TTF-TCNQ.

In the present paper, we report positron 2D-ACAR experiments on TTF-TCNQ in three different planes: b-c^*, a-c^*, and a-b, where c^* is one of the reciprocal lattice vectors (the asterisk is used for the reciprocal lattice vectors). In the first and the last planes, Fermi-surface-related structures are expected to appear since one-dimensional Fermi-surface sheets are thought to be perpendicular to the b axis. Theoretical simulations have been made with GAUSSIAN 94 (Ref. 6) to interpret the experimental results. In addition to the independent particle model (IPM), the local density approximation (LDA) and the generalized gradient approximation[7,8] (GGA) have been used to include electron-positron correlations in the calculation of the 2D-ACAR spectra. Experimental and calculational results are compared and discussed with respect to the electronic structure and the fermiology.

II. EXPERIMENT

We used the ^{22}Na isotope as the source of positrons. The nominal activity was 30 mCi (1.1 GBq). The sample was exposed to the flux of the positrons guided by a magnetic field of 2 T. When the positrons enter in the sample, they thermalize within a time of 10^{-12} s, much smaller than their lifetime [$(2–3)\times10^{-10}$ s]. Once the thermal equilibrium is reached, the positrons have the time to diffuse in the lattice before annihilating with an electron. Their positive charge drives them in the interstitial regions and, in the case of ionic systems, around the negative ions. Hence, the positrons annihilate predominantly with the valence and conduction electrons, which are the main cause of the electronic properties of the solid.

The most frequent annihilation process leads to the simultaneous emission to two γ rays. The conservation of energy during the annihilation imposes that the energy of the γ rays carries out the mass of the annihilated pair of particles, namely, 2×511 keV. The conservation of momentum im-

plies that the two γ rays fly almost in opposite directions. But there is no relation between this direction and the direction of the momentum of the annihilated pair. The amount of momentum along the direction of the γ rays gives rise to a small Doppler shift, which affects slightly their energies. This effect can also be used to study electronic properties. It is called Doppler broadening but it has a poor resolution compared to the angular correlation. We use this latter technique, which focuses on the amount of momentum $\boldsymbol{p}$ in the plane perpendicular to the direction of the γ rays. This momentum leads to a small deviation $\boldsymbol{\tau}$ from the colinearty of the two γ rays. $\boldsymbol{\tau}$ and $\boldsymbol{p}$ are directly proportional: $\boldsymbol{\tau}=\boldsymbol{p}/m_0c$, where m_0 is the rest mass of the electron and c the speed of the light in vacuum. The order of magnitude of $\boldsymbol{\tau}$ is a few mrad. A typical 2D-ACAR experiment consists of measuring the distribution of these angles in a domain of ± 30 mrad.

In the 2D-ACAR experiment, one uses a pair of planar position-sensitive detectors located on both sides of the sample to detect in coincidence the annihilation radiation (the pairs of γ rays). The ^{22}Na source is screened, so one records only the annihilations occurring in the sample. The direction of the line determined by the two detectors fixes the axis of the spectrometer. The annihilation radiation emitted only in this direction is recorded. As the lack of energy resolution of the detectors prevents detecting the Doppler shift, the 2D-ACAR experiment provides a two-dimensional projection of the (three-dimensional) TPMD, in the direction defined by the axis of the spectrometer. By changing the position of the sample in the spectrometer, one can record different projections.

The 2D-ACAR measurements were performed at 300 K with the spectrometer described in (Ref. 9). Three data sets were obtained with directions of projection along the a, b, and c^* axes. The specimen was a single crystal of 10 mm$\times$2 mm$\times$0.05 mm for the former two directions and of 7 mm $\times$1.5 mm$\times$0.05 mm for the third one. The magnitude of the reciprocal lattice vectors a^*, b^*, and c^* are 2.04, 6.35, and 1.36 mrad, respectively. At the measurement temperature, the overall resolution has a full width at half maximum of 0.9 ± 0.1 mrad. The a projection was also measured at 100 K to enhance the resolution up to 0.7 ± 0.1 mrad, by reducing the residual Brownian motion of the positron. To observe the Fermi-surface break perpendicular to the b^* axis, this resolution is acceptable, since the width of the Brillouin zone along this axis is 6.35 mrad and that of the two Fermi-surface sheets is 1.75 mrad (the position of the Fermi-surface sheets is described in the next section). Depending on the measurement, $(1.65–2.90)\times10^8$ coincidences were accumulated in histograms with a mesh of 0.15 mrad$\times$0.15 mrad. As the solid angle covered by the detectors is small, the time required to measure each 2D-ACAR distribution was about 2 weeks.

After completing the measurements, we performed the three following operations: (1) Each raw 2D-ACAR was corrected with the measured angular efficiency of the spectrometer. (2) As a consequence of the symmetry of the lattice, the 2D-ACAR distributions are also symmetric. The highest symmetries are obtained for projections along the principal crystallographic directions. This means that during the measurement, the same information is independently recorded more than once. We have checked that our 2D-ACAR exhibited the symmetries required by the lattice group of the sample. Then we folded the distribution according to their respective symmetries. This operation increases the statistical precision of our data. (3) As we have set the bin mesh of the histograms to a value much smaller than the resolution of the spectrometer, it is legitimate to sum the contents of adjacent bins. This can be viewed either as a smoothing (without degradation of the information as long as the width of the smoothing function is narrower than the resolution—it was 0.60 mrad in our case) or as an interpolation between statistically independent points.

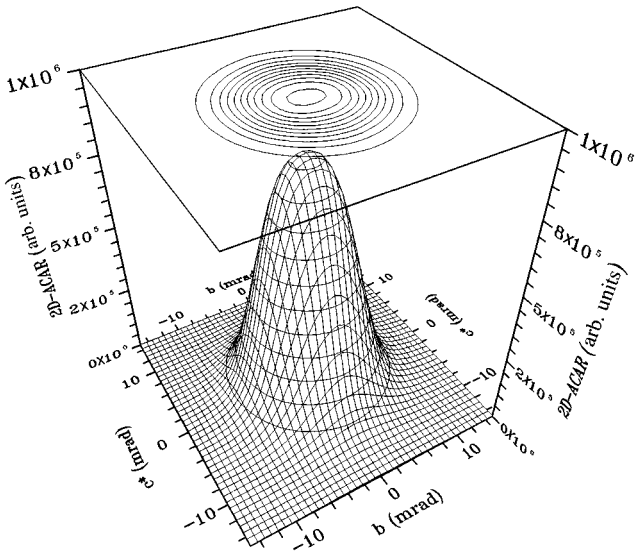

FIG. 1. The 2D-ACAR distribution measured in the b-c^* plane of TTF-TCNQ.

The 2D-ACAR distributions are bell-shaped distributions with a high degree of cylindrical symmetry as shown in Fig. 1. This feature is common when the lattice cell contains many atoms and comes from the fact that many electronic bands contribute. A good example is given by 2D-ACAR measured in high-T_c superconductors.[10] A useful way to emphasize the differences between 2D-ACAR's is to look to the anisotropic parts. We use this method here. If $N(r,\theta)$ denotes the 2D-ACAR where r and θ are the polar coordinates in the momentum plane of the distribution, the anisotropy $A(r,\theta)$ is given by

$$A(r,\theta)=N(r,\theta)-M(r), \tag{1}$$

where $M(r)$ is the mean value of $N(r,\theta)$ over θ for a given r:

$$M(r)=(1/2\pi)\int_0^{2\pi}N(r,\theta)\,d\theta. \tag{2}$$

Anisotropies of the 2D-ACAR permit to enhance the discontinuities of the electronic momentum distribution occurring with the states change of occupation.

III. CALCULATION

The electronic structure of TTF-TCNQ is expected to be well described with molecular orbitals of constituent TTF

and TCNQ due to its molecular crystal nature. In fact, the extended Hückel method, which is a simple way to obtain molecular-orbital coefficients, gives reasonably good band parameters to reproduce experimentally obtained Fermi surfaces in a similar class of materials such as TMTSF or BEDT-TTF salts.[4] Slater atomic orbitals are usually used as a basis in this method. We used more flexible basis sets in the present work, since details in the shape of wave functions are reflected on the 2D-ACAR. In addition, more precise self-consistent Hartree-Fock calculations have been performed instead of the extended Hückel method in which the matrix elements of the Hamiltonian are empirically determined.

Our calculation involves different steps from the molecular orbitals to the 2D-ACAR distributions. We shall describe them in chronological sequence.

In the first stage, we obtained molecular orbitals of the neutral TTF and TCNQ (TTF^0 and $TCNQ^0$) in terms of linear combination of atomic orbitals coefficients with GAUSSIAN 94.[6] In addition to the minimal STO-3G basis set,[11] which is obtained by expanding the Slater atomic orbital (STO) with three Gaussian functions and was used in the previous work,[12] we have tested the 3-21G,[13] 6-31G,[14] 6-31G,*[15] and 6-31G** (Ref. 15) basis sets on GAUSSIAN 94 (Ref. 6) to improve the precision and to examine the basis-set dependence.

The amount of charge transfer between TTF and TCNQ has been determined by Kagoshima, Ishiguro, and Anzai[3] to be 0.55 electrons per molecule at room temperature. In terms of molecular orbitals, 0.55 electrons are transferred from the highest occupied molecular orbital (HOMO) of TTF^0 to the lowest unoccupied molecular orbital (LUMO) of $TCNQ^0$.

In the second stage, after taking this charge transfer into account, values of the Coulombic potential, the electronic charge density, and the electron-positron correlation potential were calculated to construct the potential for positrons on a three-dimensional grid of $61 \times 21 \times 91$ points, which was set up on the crystal unit cell (points on the boundary are shared with neighboring cells). The mesh spacings were ~ 0.2 Å in the present case. Orbital relaxations due to the charge transfer were ignored. It is thought that the charge transfer causes a significant change of the energy eigenvalue for each orbital but less in the shape of the wave function. In fact, the simulated 2D-ACAR spectra are not changed significantly if we use the molecular orbitals of TTF^{2+} and $TCNQ^{2-}$ to express the electron wave functions. The electron-positron correlation term of the potential was expressed by two different electronic density functionals: one by Boroński and Nieminen[16] in the LDA and the other by Barbiellini *et al.*[7,8] in the GGA.

In the third stage, the positron wave function was obtained with the finite-difference method.[17] At this stage, we have the electronic wave functions ψ_{-j} (j is the molecular-orbital index) and the positron wave function ψ_+.

Next, in the fourth stage, we extended the grid to $256 \times 256 \times 256$ points. The center of the TTF or TCNQ molecule (in the crystal coordinates (0, 0, 0) and (1/2, 0, 0), respectively) corresponds to that of the grid. Values of the product $\psi_{-j}\psi_+$ were calculated on the grid points (x,y,z). By applying three-dimensional fast Fourier transformation, a partial TPMD spectrum $\rho_j^{2\gamma}$ was obtained for each molecular orbital j as

$$\begin{aligned}\rho_j^{2\gamma}(x',y',z') &= \text{const}\left| \int d\boldsymbol{r}\, \exp(-i\boldsymbol{pr}) \right. \\ &\quad \left. \times \psi_{-j}(\boldsymbol{r})\psi_+(\boldsymbol{r})\sqrt{\gamma(\boldsymbol{r})}\right|^2 \\ &= \text{const}\left|\text{FFT}[\psi_{-j}(x,y,z)\psi_+(x,y,z) \right. \\ &\quad \left. \times \sqrt{\gamma(x,y,z)}]\right|^2, \end{aligned} \tag{3}$$

where (x',y',z') represents each grid point in the momentum space. $\gamma(x,y,z)$ is the enhancement factor, describing the enhancement of the electronic density around the positron due to the electron-positron correlation, at the point (x,y,z) of the crystal lattice space. In the IPM, its value is always unity (we used the positron wave function obtained with the LDA correlation potential in calculating the IPM 2D-ACAR spectra). For the LDA or GGA, we used the expression by Boroński and Nieminen[16] and that by Barbiellini *et al.*,[7,8] respectively.

In the fifth stage, we calculated the 2D-ACAR spectra $\rho_{2D}^{2\gamma}$ corresponding to the experiments by summing the partial TPMD spectra over the orbitals j and integrating along the a, b, and c^* axes (parallel to the x', y', and z' directions, respectively):

$$\rho_{2D}^{2\gamma}(y',z') = \text{const} \times \sum_j \int dx' n_j \rho_j^{2\gamma}(x',y',z'), \tag{4}$$

$$\rho_{2D}^{2\gamma}(x',z') = \text{const} \times \sum_j \int dy' n_j \rho_j^{2\gamma}(x',y',z'), \tag{5}$$

$$\rho_{2D}^{2\gamma}(x',y') = \text{const} \times \sum_j \int dz' n_j \rho_j^{2\gamma}(x',y',z'). \tag{6}$$

All occupied orbitals were included. There are 52 occupied orbitals for the TTF molecule and 53 for TCNQ. Two TTF and two TCNQ molecules exist in the crystal unit cell. One TTF or TCNQ molecule can be superposed on the other one by a screw operation.

The band occupation number n_j is always 2 except the HOMO of TTF^0 and the LUMO of $TCNQ^0$. As mentioned above, these two orbitals are only partially occupied due to

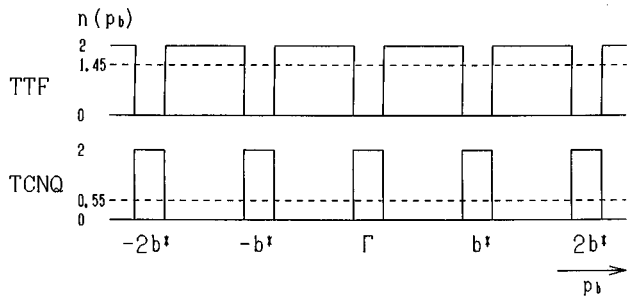

FIG. 2. Occupation numbers for HOMO-TTF^0 and LUMO-$TCNQ^0$ along the b^* direction for the models without Fermi surface (dashed line) and with Fermi surface (solid line).

the charge transfer. In order to take into account this effect, we have used two models. One is to set

$$n_{\text{HOMO-TTF}^0} = 2 - 0.55 = 1.45 \tag{7}$$

$$n_{\text{LUMO-TCNQ}^0} = 0.55. \tag{8}$$

This model describes the case where no Fermi surface is present.

The second model includes the Fermi surface. The position of one-dimensional Fermi-surface sheets can be estimated from the charge-transfer value of 0.55 to be $(\pm 0.55/4+n)b^*$, where n is an integer and b^* is a reciprocal lattice vector parallel to the b axis.[3] Accordingly, $n_{\text{HOMO-TTF}^0}$ and $n_{\text{LUMO-TCNQ}^0}$ have been represented as functions of y':

$$n_{\text{HOMO-TTF}^0}(y') = \begin{cases} 0 & \text{if } (-0.55/4+n)b^* < y' < (+0.55/4+n)b^* \\ 2 & \text{otherwise,} \end{cases} \tag{9}$$

$$n_{\text{LUMO-TCNQ}^0}(y') = \begin{cases} 2 & \text{if } (-0.55/4+n)b^* < y' < (+0.55/4+n)b^* \\ 0 & \text{otherwise.} \end{cases} \tag{10}$$

The Fermi-surface position is the same for both the TTF and TCNQ chains and, as shown in Fig. 2, the highest TTF band is unoccupied in the k-space region where the highest TCNQ band is occupied and vice versa. Since positrons are distributed around TCNQ more than around TTF, as will be shown below, the electron ridge Fermi surface due to the LUMO of $TCNQ^0$ is sampled with a higher probability and a signal can be observed in the 2D-ACAR. By comparing the results of these two models, we can investigate Fermi-surface effects on 2D-ACAR spectra.

In the sixth and final stage, calculated 2D-ACAR spectra were convoluted with the experimental resolution function. The resulting spectra are bell shaped like the experimental ones. The anisotropic parts were extracted in the same way that has been done for the experimental distributions so that they can be directly compared.

The 2D-ACAR calculations in the IPM were performed with five different basis sets (STO-3G, 3-21G, 6-31G, 6-31G*, and 6-31G**). The accuracy is expected to increase in this order, because the number of Gaussian functions for core electrons and the flexibility to express valence electrons increase. Though the 6-31G basis set is accurate enough, as mentioned in the next section, we have made calculations in the LDA and GGA with the 6-31G** basis set, which is thought to be the most accurate among the basis sets utilized in the present work.

IV. RESULTS AND DISCUSSION

Figures 3(a)–3(c), left panels, show the experimental 2D-ACAR anisotropies on TTF-TCNQ in the b-c^*, a-c^*, and a-b planes, respectively (right panels are theoretically simulated ones, which will be described later). These anisotropies were obtained according to Eqs. (1) and (2). Their maximum amplitude is 2–4% of the peak height of the spectra. These values are very similar to those obtained for the high-

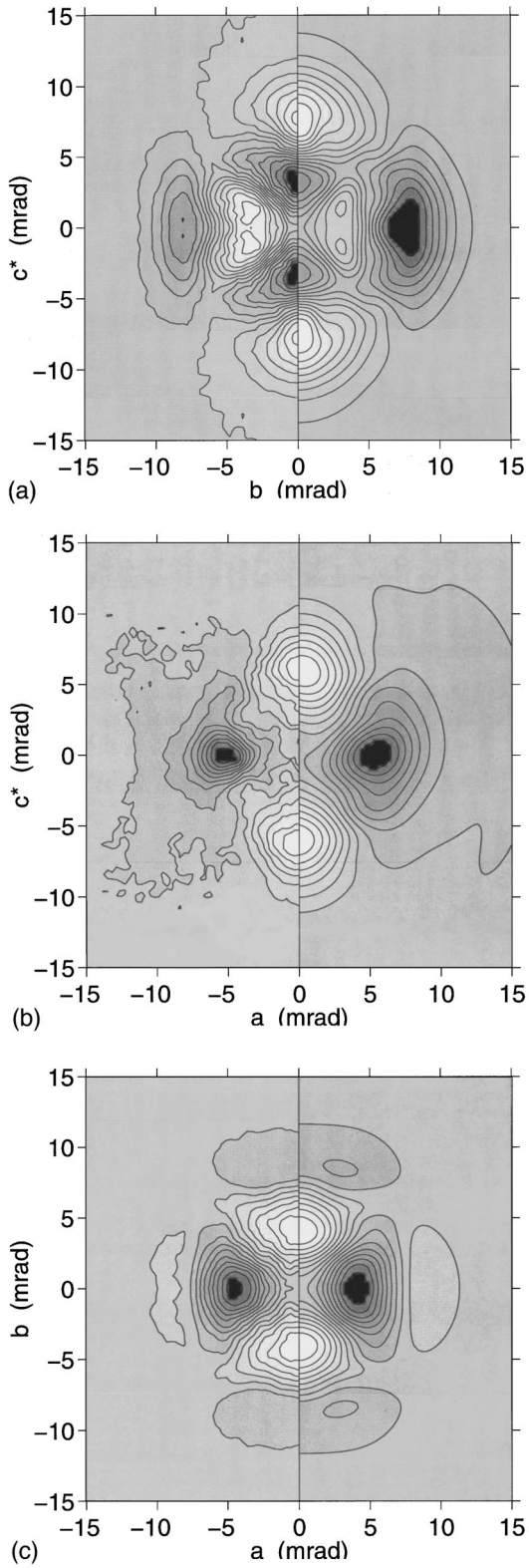

FIG. 3. Anisotropy of the 2D-ACAR distributions in the (a) b-c^*, (b) a-c^*, and (c) a-b planes. Left panels: experiment; right panels: calculated within GGA and with a charge transfer of 0.7 electrons. White is high and black is low.

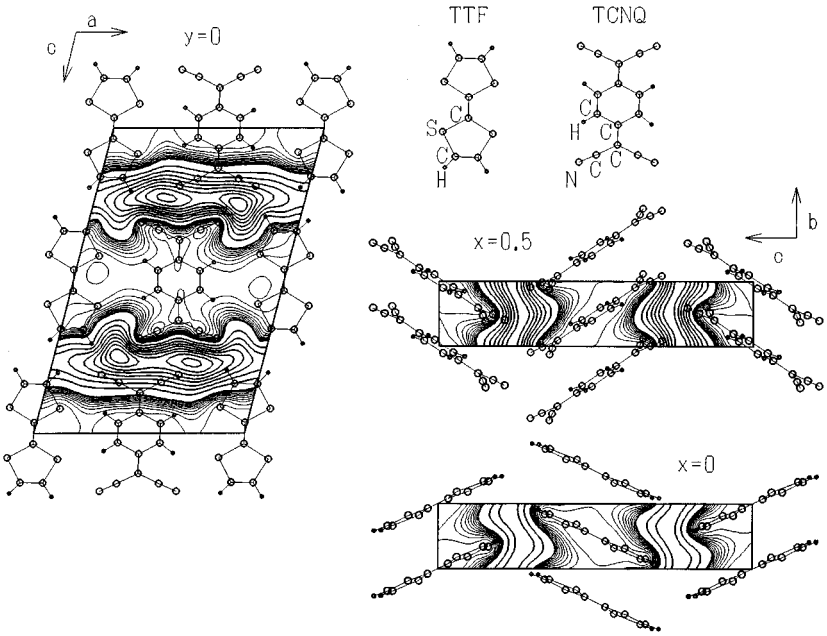

FIG. 4. Positron density distribution in the TTF-TCNQ crystal calculated with the 6-31G** basis set in the GGA [the contours are in steps of 0.01 from 0.01 to 0.09 (thin lines) and steps of 0.1 from 0.1 to 0.9 (thick lines), where the maximum value is normalized as unity].

temperature superconducting oxides.[10] Observed anisotropies are determined by Fermi-surface and wave-function effects. In the following, we interpret them by comparing with the theoretical simulations.

First, let us mention the positron distribution in the TTF-TCNQ crystal. The basis-set dependence of the positron density distribution calculated in the LDA has been already reported.[18] The 6-31G, 6-31G*, and 6-31G** basis sets give similar results, in which positrons are distributed quasi-two-dimensionally and the density has peaks around the CN groups of the TCNQ molecule. The distribution for the STO-3G is more localized between the CN groups of TCNQ while that for the 3-21G has the maximum between TTF columns. These two basis sets seem to be insufficient to describe properly the electronic charge density. The result for 6-31** in the GGA is shown in Fig. 4 together with the crystallographic view. The LDA result is similar to this one.[18,19]

In Figs. 5(a)–5(c), we show the 2D-ACAR anisotropies in the b-c^*, a-c^*, and a-b planes calculated with the 6-31G** basis set in the GGA, which are thought to be most accurate. Left panels are without the Fermi surface [Eqs. (7) and (8)] while right panels contain the Fermi surface described by Eqs. (9) and (10). If we compare the right panels with the left ones, it is observed that the presence of the Fermi breaks gives small differences in the b-c^* plane [Fig. 5(a)] and in the a-b plane [Fig. 5(c)]. Additional structures appear in the Fermi-surface (FS) case. In the right panel of Fig. 5(a), there are neck structures at $p_b = \sim 1$ mrad and $p_{c^*} = 5$–7 mrad, which correspond to the estimated position of the Fermi surface at $p_b = (0.55/4)b^* = 0.874$ mrad. Around $p_b = 6$ mrad, there are other structures, which are due to the Fermi surface in the second Brillouin zone. In the right panel of Fig. 5(c), there are hornlike structures at the same position $p_b = 6$ mrad. The anisotropy in the a-c^* plane [Fig. 5(b)] shows little difference between the two cases. It is quite reasonable because Fermi surfaces are parallel to this plane and do not induce breaks in this 2D-ACAR distribution. The common structures in the left and right panels are thought to be due to the fully occupied orbitals but it is not straightforward to assign them to the specific contribution of one particular orbital as anisotropies from more than 100 orbitals add together to give the observed spectra.

If we compare the experimental results in Fig. 3 left panels with the calculated ones in Fig. 5, we find that the overall agreement is fairly good. The Fermi-surface-related structures discussed above are also observable as necks and horns in the experimental 2D-ACAR spectra in Figs. 3(a) and 3(c), respectively. It is noticeable that the Fermi surface can be observed despite the fact that the occupancies of the topmost orbitals of TTF and TCNQ compensate each other in k space as shown in Fig. 2. One reason, which is thought to be significant, is that positrons probe electrons of TCNQ more than those of TTF, as shown in Fig. 4, since the TCNQ molecule (the CN groups) is negatively charged. The present calculation of the positron wave function predicts this. As a result, the Fermi breaks due to the topmost TCNQ band are more pronounced. The other reason is that there is a strong wave-function effect. Molecular orbitals are far from homogeneous in the real space and large modulations of electronic densities in the k space are expected. The difference in the modulations of the highest orbitals between TTF and TCNQ results in discontinuities at the Fermi wave numbers.

We would like to mention our finding that the agreement between the experiment and the simulation can be improved if we assume a slightly larger charge-transfer amount than the value of 0.55 reported by Kagoshima, Ishiguro, and Anzai,[3] which is thought to be the most accurate value. In the present calculations, the charge-transfer amount is the only value that can be treated as an adjustable parameter. For reference, the amount of the charge transfer was determined by the numerical integration of x-ray diffraction amplitudes to be $(0.48$–$0.60) \pm 0.15$ (at 100 K) (Ref. 20) or by the x-ray photoemission spectroscopy to be 0.57–0.67.[21] In Fig. 3, right panels, the obtained spectra with the charge transfer of 0.7 in the FS case are shown to compare to the experimental

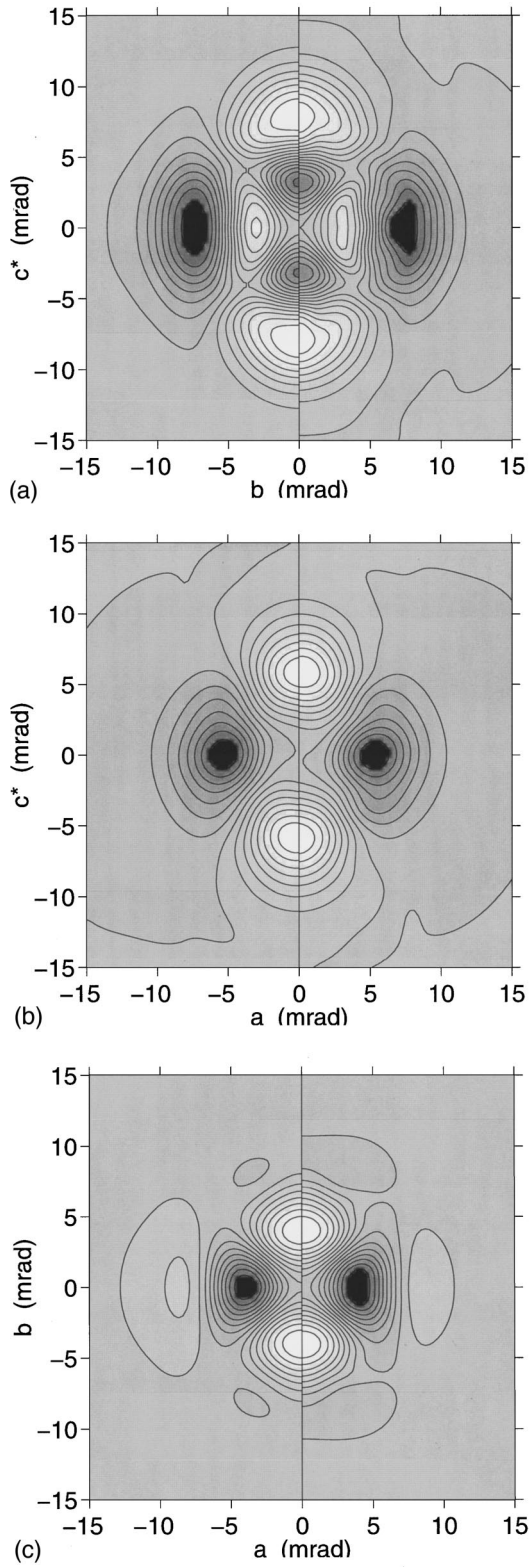

FIG. 5. Anisotropy of the 2D-ACAR distributions calculated with GGA in the (a) b-c^*, (b) a-c^*, and (c) a-b planes. Left panels: without Fermi surface; right panels: with Fermi surface and a charge transfer of 0.55 electrons. White is high and black is low.

ones. They reproduce the experimental spectra better than those in Fig. 5, obtained with a charge transfer of 0.55. The increase of the charge transfer causes two effects in the calculational results. One is that positrons are gathered more around negatively charged TCNQ molecules. The other is that the position of the Fermi surface is shifted (in the first Brillouin zone, toward a higher momentum). The former effect enhances the Fermi-surface break because positrons sample the electron surface due to TCNQ much more than the hole surface due to TTF. The latter effect broadens the width of the ridgelike Fermi surface. From our positron experiment, the charge transfer seems to be slightly overestimated. The screening of the positron by the valence electrons might be at the origin of this apparent increase of the charge transfer: as we know from the calcuation of the positron wave function, the positrons are predominantly located around the TCNQ molecule. The screening of the positron will enhance the electron transferred from the HOMO of TTF (the energetically most easy source of electrons) to the LUMO of TCNQ. Nevertheless, it is unclear if this effect can modify the position of the Fermi surface because the screening of the positron extends in a small region while the Fermi surface is a large-scale consequence of the electronic struture in the periodic crystal structure.

Let us briefly discuss the basis-set dependence in the IPM calculations. The minimal STO-3G basis set reproduces relatively well the experimental 2D-ACAR anisotropy in the a-c^* plane, as already shown.[12] For the other directions, the agreement is found to be poor, however. We can improve the agreement with the experiment by introducing the 3-21G set but it is still not enough. As mentioned above, the positron distribution obtained with these basis sets is inaccurate. This is the main reason for the poor agreement. For the 6-31G, 6-31G*, and 6-31G** sets, the results are quite similar. This is also the same for the positron distributions. We may expect that the 6-31G basis set works well for a similar class of materials.

We have compared the IPM, LDA, and GGA results obtained with the 6-31G** basis set. In the IPM, as its name implies, the interaction between a positron and electrons is neglected. In the LDA, in contrast with this, a positron is thought to be surrounded by a screening electron cloud. With the electron density decreasing, the relative magnitude of the screening to the local electron density increases. The GGA interpolate these two extremes.[7,8] These features are reflected on the calculated results. For the IPM results, the overall agreement with the experiment is rather good but poorer than that for the GGA results. The extent of anisotropy contours is significantly larger than the experimental one (and the GGA one). The reason would be that, in the IPM, positrons are thought to probe lower-momentum valence electrons and higher-momentum core electrons equally. In fact, positrons are more sensitive to valence electrons. The GGA results are better than the IPM ones on the shape and the relative magnitude of the peaks as well as the dips. The difference between the results of the LDA and GGA is small though the latter reproduce the experimental anisotropies slightly better. Among the three approximations used in the present work, the GGA is the best to reproduce the experimental results. According to Barbiellini *et al.*,[7,8] the GGA is not applicable to a very low electron density system/region, e.g., surface. As for the present material TTF-TCNQ, though the electron density is rather low in the interstitial region [the lowest density corresponds to a density parameter value of $r_s=(3/4\pi n)^{1/3}=8.2$], the GGA seems to work well.

Three other analyses have been performed in order to attempt more precise indentifications of the Fermi-surface signatures. The Lock-Crisp-West (LCW) folding[22] has been applied to the measured and calculated 2D-ACAR spectra. It is known that the LCW folding enhances the breaks induced by the Fermi surface if the positron wave function is homogeneous in the crystal lattice cell. This condition is far from fulfilled in TTF-TCNQ, as can be seen from Fig. 4. In fact, after the LCW folding, it is hard to distinguish our two calculated spectra though one has no Fermi surface and the other has the Fermi surface. Therefore, the LCW folding technique does not provide extra information about the Fermi surface. In our opinion, one should also be very careful about conclusions drawn on the basis of LCW foldings in other organic metals.[23,24] The two other analyses are the enhancement of Fermi-surface images[25] and a filtering technique based on the principle of the maximum entropy.[26] No conclusive results have been obtained from these analyses. The signals of the Fermi surface seem too small. A slight improvement of the resolution by measuring at 100 K did not result in a significant difference.

Measurements with higher momentum resolution and larger statistics than those used in this work are required. They would only be possible with a high-intensity positron beam.[27] Another benefit would be the reduction of radiation damage. Indeed, we cannot exclude radiation damage by high-energy positrons from our ^{22}Na source. It might create defects able to trap a fraction of positrons, reducing the amplitude of the signals from the Fermi surface. Measurements of the positron lifetime[18,19] do not exclude effects of radiation damage in the 2D-ACAR measurements since a positron beam with much lower intensity and energy was used in the lifetime measurements. So far, no definite picture is obtained for defects and positron trapping in TTF-TCNQ.

V. CONCLUSION

We have measured positron 2D-ACAR distributions on TTF−TCNQ and extracted their anisotropies. We have also performed a theoretical simulation based on *ab initio* molecular orbital calculations. The overall agreement between the experimental and calculated anisotropies is good and it has been improved by including the electron-positron correlation within the LDA or GGA formalism. This shows that positron 2D-ACAR is an appropriate method for the study of the electronic structure of organic conductors. The presence of the Fermi-surface breaks causes small but significant additional structures on the simulated 2D-ACAR spectra in the b-c^* and a-b planes. The experimental anisotropies in these planes are consistent with such structures and suggest a charge transfer higher (0.7 electrons) than the value of 0.55 obtained from the Kohn anomaly.[3]

ACKNOWLEDGMENTS

The authors are grateful to Professor M. Peter and Professor Ø. Fischer for their continuous encouragements, to Professor D. Jérome and to Dr. M. Tokumoto, Dr. Y. Tanaka, Dr. H. Katagiri, and Dr. B. Barbiellini for helpful discussions. We thank Dr. D. Vasumathi for her careful reading of the manuscript. All the calculations were performed on the CRAY;C90 system at the Research Information Processing System/Station (RIPS) center, the Agency of Industrial Science and Technology (AIST), the Ministry of International Trade and Industry (MITI).

[1] T.J. Kistenmacher, T.E. Phillips, and D.O. Cowan, Acta Crystallogr. B **30**, 763 (1974).

[2] M.J. Cohen, L.B. Coleman, A.F. Garito, and A.J. Heeger, Phys. Rev. B **10**, 1298 (1974).

[3] S. Kagoshima, T. Ishiguro, and H. Anzai, J. Phys. Soc. Jpn. **41**, 2061 (1976).

[4] J. Wosnitza, *Fermi Surfaces of Low-dimensional Organic Metals and Superconductors* (Springer, Berlin, 1996).

[5] *Positron Spectroscopy of Solids*, edited by A. Dupasquier and A.P. Mills, Jr. (IOS, Amsterdam, 1995).

[6] M.J. Frisch, G.W. Trucks, H.B. Schlegel, P.M.W. Gill, B.G. Johnson, M.A. Robb, J.R. Cheeseman, T. Keith, G.A. Petersson, J.A. Montgomery, K. Raghavachari, M.A. Al-Laham, V.G. Zakrzewski, J.V. Ortiz, J.B. Foresman, C.Y. Peng, P.Y. Ayala, W. Chen, M.W. Wong, J.L. Andres, E.S. Replogle, R. Gomperts, R.L. Martin, D.J. Fox, J.S. Binkley, D.J. Defrees, J. Baker, J.P. Stewart, M. Head-Gordon, C. Gonzalez, and J.A. Pople, GAUSSIAN 94, Revision B.3 (Gaussian, Inc., Pittsburgh, PA, 1995).

[7] B. Barbiellini, M.J. Puska, T. Torsti, and R.M. Nieminen, Phys. Rev. B **51**, 7341 (1995).

[8] B. Barbiellini, M.J. Puska, T. Korhonen, A. Harju, T. Torsti, and R.M. Nieminen, Phys. Rev. B **53**, 16 201 (1996).

[9] P.E. Bisson, P. Descouts, A. Dupanloup, A.A. Manuel, E. Perréard, M. Peter, and R. Sachot, Helv. Phys. Acta **55**, 100 (1982).

[10] L.C. Smedskjaer R. Pankaluoto, A. Bansil, and P.E. Mijnarends, J. Phys. Chem. Solids **54**, 1239 (1993).

[11] W.J. Hehre, R.F. Stewart, and J.A. Pople, J. Chem. Phys. **51**, 2657 (1969).

[12] S. Ishibashi, A.A. Manuel, and L. Hoffmann, J. Phys. Chem. Solids **56**, 1955 (1995).

[13] J.S. Binkley, J.A. Pople, and W.J. Hehre, J. Am. Chem. Soc. **102**, 939 (1980).

[14] W.J. Hehre, R. Ditchfield, and J.A. Pople, J. Chem. Phys. **56**, 2257 (1972).

[15] P.C. Hariharan and J.A. Pople, Theoret. Chim. Acta (Berlin) **28**, 213 (1973).

[16] E. Boroński and R.M. Nieminen, Phys. Rev. B **34**, 3820 (1986).

[17] M.J. Puska and R.M. Nieminen, J. Phys. F **13**, 333 (1983).

[18] S. Ishibashi, M. Tokumoto, N. Kinoshita, N. Terada, H. Ihara, R. Suzuki, T. Ohdaira, T. Mikado, and H. Anzai, Can. J. Phys. **74**, 534 (1996).

[19] S. Ishibashi, M. Tokumoto, N. Kinoshita, N. Terada, H. Ihara, R. Suzuki, T. Ohdaira, T. Mikado, and H. Anzai, Appl. Surf. Sci. (to be published).

[20] P. Coppens, Phys. Rev. Lett. **35**, 98 (1975).

[21] W.D. Grobman and B.D. Silverman, Solid State Commun. **19**, 319 (1976).

[22] D.G. Lock, V.H.C. Crisp, and R.N. West, J. Phys. F **3**, 561 (1973).

[23] Y.C. Jean, Y. Lou, H.L. Yen, K.M. O'Brien, R.N. West, H.H. Wang, K.D. Carlson, and J.M. Williams, Physica C **221**, 399 (1994).

[24] L.P. Chan, K.G. Lynn, D.R. Harshman, and R.C. Haddon, Phys. Rev. B **50**, 10 393 (1994).

[25] K.M. O'Brien, M.Z. Brand, S. Rayner, and R.N. West, J. Phys. Condens. Matter **7**, 925 (1995).

[26] L. Hoffmann, A. Shukla, M. Peter, B. Barbiellini, and A.A. Manuel, Nucl. Instrum. Methods Phys. Res. Sect. A **335**, 276 (1993).

[27] D. Gerola, W.B. Waeber, and M. Shi, Nucl. Instrum. Methods Phys. Res. Sect. A **364**, 33 (1995).